Nonlinear Voltage Regulation Strategy for a Fuel Cell/Supercapacitor Power Source System

Yuz A. Zúñiga-Ventura*, Diego Langarica-Córdoba†, Jesús Leyva-Ramos*
Luis H. Díaz-Saldierna*, Irwin A. Díaz-Díaz*
**División de Matemáticas Aplicadas, IPICyT*
Camino a la Presa San Jose 2055 Col. Lomas 4a. Sección,
78216. San Luis Potosí, México
E-mail: yuz.zuniga@ipicyt.edu.mx
† *School of Sciences, UASLP*
78290. San Luis Potosí, México. Email: @@@ pendiente@@@

***Abstract*—The main goal of this paper is to model and control a fuel cell/supercapacitor power source system to feed a DC-bus with a constant output voltage despite load changes. The fuel cell is modeled as a nonlinear current-dependent voltage source through a power equation meanwhile, the supercapacitor is represented as an ideal capacitor. The power converters are modeled using a nonlinear averaged model based on Kirchhoff laws. Furthermore, the proposed nonlinear state feedback control method is inspired from backstepping technique and Lyapunov stability analysis to ensure all error signals equal to zero. Also, a load estimator using Immersion-Invariance (I&I) theory to track load changes through available measurements is considered. Finally, simulation results show that the proposed control scheme stabilizes the system when sudden load changes are introduced.**

***Index Terms*—Fuel cell, supercapacitor, DC-DC power converter, nonlinear control systems.**

I. Introduction

Currently, the main form of power generation depends on fossil fuels such as oil, coal and natural gas, whose release to the atmosphere affects global warming and human health. Thus, industrial and academic communities are researching alternative sources of energy, to supply power consumption and to decrease pollutant generation as well. Nowadays, fuel cells (FC) technology has been of great interest for its ability to transform chemical energy into electrical energy [1]. Particularly, proton exchange membrane FC are remarkable for mobile and stationary applications due to its capabilities such as reduced noise pollution, low-temperature operation, high power density, low weight, and compactness [2]. Additionally, FC are more efficient and green than other power generation sources, since heat and water are the only by-products [3].

On the other hand, fuel cells output voltage presents some drawbacks such as a nonlinear dependence to electric current, temperature, pressure and humidity. Moreover, the fuel cell membrane can be degraded or damaged if the demanded current slope is significantly high in shorts periods of time [4]. For this reason dynamically fast storage devices, such as supercapacitor (SC) or battery bank, are required to supply (or absorb) electrical power surplus imposed by the demand-side. To this end, current research studies are being focused on advanced control schemes to improve accurate regulated conditions for a proper FC operation in combination with a supercapacitor bank [5]–[9] and also with a battery bank [10]–[12] for electric transportation and power distributed generation applications.

The contribution of this work relies on the combination of current-mode techniques and nonlinear feedback control to solve the output voltage regulation problem for a fuel cell/supercapacitor power conversion system. The proposed multi-loop scheme contemplates; first, an inner current loop employed to ensure a current reference tracking, and second, an outer voltage loop used to generate a proper current reference. Different from the above references, this work splits the dynamics of the system into two, current (fast) and voltage (slow). The overall strategy results in a nonlinear adaptive state feedback controller, which ensures asymptotic convergence of all error signals to the origin. Moreover, a load estimator using immersion-invariance (I&I) approach is used, to improve the robustness of the outer loop. In this way, the estimator design stage is based on the sum an integral, and a proportional term to represent the parameter estimation and it uses in a certainty-equivalent way this estimation in the control scheme [13], [14]. The proposed controller performance has been evaluated through numerical simulation, where a good output voltage regulation is observed despite sudden load changes.

The rest of this work is organized as follows. In Section II, the mathematical modeling of the multi-source is presented. The controller design and the analysis are given in Section III. Section IV presents numerical results. Finally, conclusions are given in Section V.

II. Mathematical Modeling of the Multi-Source System (MSS)

The MSS under study is shown in Fig. 1. Notice that this configurations has been considered in [5], [7], [8], [15], [16]. The FC, boost, buck-boost and output currents are represented by I_F, I_{LF}, I_{LS} and I_O, respectively. Meanwhile, the voltage in the FC, SC and in the output are represented by V_F, V_S and V_O, respectively. Additionally, L_F and L_S are converters inductors, C_F and C_O are the capacitors of the converter and

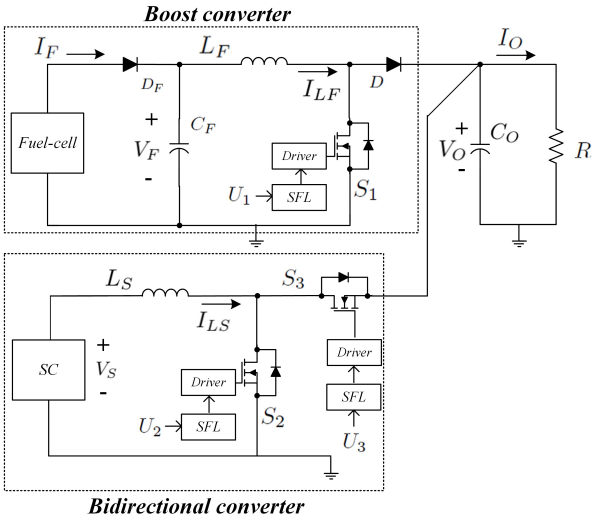

Fig. 1. Configuration of the multi-source system under study.

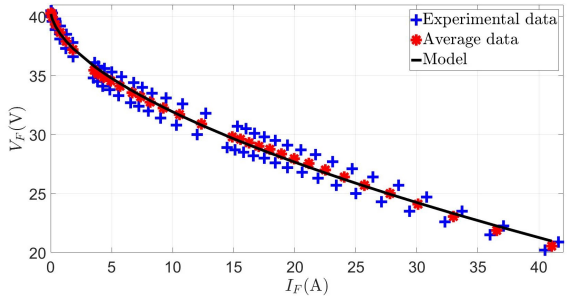

Fig. 2. Fuel cell stack polarization curve.

the output. The diode D_F is used to prevent a reverse current to the FC. U_1, U_2 and U_3 denote the control signals. Furthermore, switching frequency limiters (SFL) and gate drivers are used to commute the switches S_1, S_2 and S_3 of the converters. In the present case, a DC-bus is supplied by an FC (main source) through a conventional boost converter. Furthermore, an SC bank is used as an auxiliary source to supply fast transient power demand. To this end, a bidirectional "buck-boost" converter is used. Finally, it is assumed that the DC-bus feed a purely resistive load R.

A. Fuel cell stack characteristics

As stated before, the FC output voltage depends in a nonlinear fashion on the demanded current. This behavior can be observed in Fig. 2, where the static V-I experimental polarization curve of the 1.2 kW Nexa FC under study is presented. Detailed mathematical descriptions using high-order nonlinear models for thermal and chemical dynamical behavior have been reported in the literature [2], [17], [18]. For feedback purpose, a simple FC stack model with electric properties compatible with power conversion is used in this work. For instance, a static expression for the output voltage, V_F, depending on the current, I_F, is described by a two-termed nonlinear power function as

$$V_F(I_F) = a{I_F}^b - c \tag{1}$$

where a, b and c are constants to be computed. In particular, based on experimental data, these constants can be approximated using a logarithmic transformation and a linear regression of the averaged data [19]. Consider that, (2), holds true for use in a dynamic condition present in the boost converter operation. A similar expression has been used in previous work [20]. Note that, Fig. 2 shows a comparison between experimental data and the expression in (1), where the accuracy of the method is confirmed. Additionally, this static model provides a nonlinear characterization that satisfactorily describes the FC stack behavior, successfully covering the entire operation range of the fuel cell-based system, including the three major losses, namely, activation, ohmic, and transport [5]. For control purposes, other static models representing the $V-I$ polarization curve characteristics of a given stack have been proposed in [15], [16], [20], [21]; however, the static model (1) is more simple, since it only uses three parameters, i.e., a, b and c, which could be obtained easily from the aforementioned method.

B. Energy Management Strategy

For the MSS, four different operation modes are identified from the literature [5]. These are summarized as follows:

- **Delivery mode** occurs when the main source supplies power to the load during MSS steady state. Thus, the signal $U_2 = U_3 = 0$.
- **Support mode** is present when the supercapacitor provides energy to the load during a power transient. Consequently, $U_3 = 0$ (Boost mode).
- **Charge mode** arise after support mode is finished. In this case, the main source supplies power to the storage device and load simultaneously. Therefore, $U_2 = 0$ (Buck mode).
- **Recovery mode** takes place when the load supplies power to the storage device. Finally, $U_2 = 0$ (Buck mode).

The main objective of the MMS is to provide accurate DC-bus voltage regulation, despite load changes and ensuring smooth variations of the FC current to avoid a lifetime degradation. The last is assured by the design of two feedback control loops, namely an inner loop for current tracking and an outer loop for voltage regulation (see Fig. 3). It is important to remark that the SC current reference is positive in the support (boost) mode and negative in the charge (buck) mode [5].

C. Overall mathematical model of the system

The dynamic behavior of the system is represented by a set of nonlinear differential equations that captures the average value of the electrical variables and neglects the ripple effect caused by the switching action. Such model is obtained from

current and voltage Kirchhoff laws when the switches are ON/OFF, in this way, the MSS is represented by

$$\begin{aligned} C_F\dot{V}_F &= \left(\frac{V_F - c}{a}\right)^{1/b} - I_{LF}, \\ L_F\dot{I}_{LF} &= V_F - V_O(1-U_1), \\ C_S\dot{V}_S &= -I_{LS}, \\ L_S\dot{I}_{LS} &= V_S - V_O U_{23}, \\ C_O\dot{V}_O &= I_{LF}(1-U_1) + I_{LS}U_{23} - I_O, \end{aligned} \tag{2}$$

where V_F, I_{LF}, V_S, I_{LS} and V_O are the state variables. Moreover $U_{23} = (1-U_2)k + U_3(1-k)$ represents an auxiliary control signal, related to the pulse-width modulation (PWM) duty cycles U_1 and U_2. Notice that, k is a binary signal which defines the *boost mode* of the bidirectional (Bd) converter when $k = 1$ and *buck mode* when $k = 0$. In this work, the mathematical model (2) was obtained based on the following assumptions:

- The state variables are measurable, and all parameters are known except the load R.
- The system is operating under continuous conduction mode.
- All passive elements are considered ideal.

In practice, these assumptions are unrealistic; nevertheless, they are extensively used to simplify the control design stage.

In steady state, providing that the control signal remains constant, i.e., $U_1 = \bar{U}_1$ and $U_{23} = \bar{U}_{23}$, the average output voltage $\bar{V}_O$ is greater than the input $\bar{V}_F$ and $\bar{V}_S$, also the inductor current $\bar{I}_{LF}$ equals to the fuel cell current $\bar{I}_F$, therefore the operating points of (2) are found to be

$$\begin{aligned} \bar{V}_O &= \frac{\bar{V}_F}{(1-\bar{U}_1)}, \\ \bar{V}_S &= \bar{U}_{23}\bar{V}_O, \\ \bar{I}_{LF} &= \frac{\bar{V}_O}{R(1-\bar{U}_1)} = \left(\frac{\bar{V}_F - c}{a}\right)^{\frac{1}{b}}, \\ \bar{I}_{LS} &= 0, \end{aligned} \tag{3}$$

and once the nominal output voltage $\bar{V}_O$, the load resistance R and duty cycle $\bar{U}_1$ are defined, $\bar{V}_F$ is computed from the numerical solution of

$$\bar{V}_F(\bar{V}_O) = a\left(\frac{\bar{V}_O}{R(1-\bar{U}_1)}\right)^b + c. \tag{4}$$

Note that, in practice, the value of $\bar{V}_F$ is difficult to obtain; therefore, the control scheme needs to be designed avoiding the usage of $\bar{V}_F$.

III. Controller Design and Analysis

The proposed controller detailed in here, employs two control loops (see Fig. 3). An *inner loop* is used to generate the PWM U_1 and U_2, as well as ensures a proper current references tracking. On the other hand, an *outer loop* is used to generate the current references I^*_{LF} and I^*_{LS} required

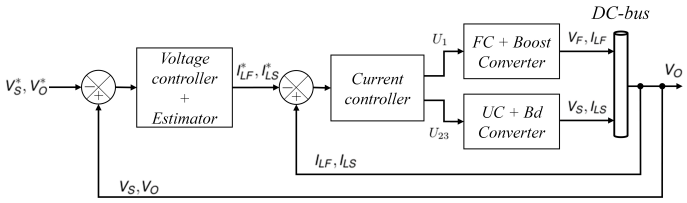

Fig. 3. Block diagram of the proposed closed-loop system.

to drive the system to desired voltage levels. Both control loops are inspired from backstepping technique and Lyapunov stability analysis. Additionally, the proposed scheme employs an adaptation law based on I&I theory to estimate the load resistance, R, where the convergence rate of the estimator is related to the slope of I^*_{LF}. FC damage can be avoided if I^*_{LF} slope is slow. Notice that, in literature, it is often assumed that the time scale between the current and voltage is significantly large; therefore, singular perturbation theory can be applied and a separation between current and voltage dynamics is possible [8]. In the sequel, the design stage is given in three parts, where the controller synthesis is fully detailed.

A. Current controller (Inner loop)

As stated before, due to the time scale differences, consider the separation between the current and voltage dynamics. In this way, the *fast* dynamics of (2) are

$$\begin{aligned} L_F\dot{I}_{LF} &= V_F - V_O(1-U_1), \\ L_S\dot{I}_{LS} &= V_S - V_O U_{23}, \end{aligned} \tag{5}$$

where the voltages V_F and V_S are considered as constants. Afterwards, define the inductor current error signals as

$$\begin{aligned} x_1 &:= I_{LF} - I^*_{LF}, \\ x_2 &:= I_{LS} - I^*_{LS}. \end{aligned} \tag{6}$$

Consequently, the error dynamics of (5) are

$$\begin{aligned} \dot{x}_1 &= \frac{V_F}{L_F} - (1-U_1)\frac{V_O}{L_F} - \dot{I}^*_{LF}, \\ \dot{x}_2 &= \frac{V_S}{L_S} - U_{23}\frac{V_O}{L_S} - \dot{I}^*_{LS}. \end{aligned} \tag{7}$$

Observe that, if the control signals are selected as

$$\begin{aligned} U_1 &= 1 + \frac{1}{V_O}\left[L_F(-\alpha_1 x_1 + \beta x_2 + \dot{I}^*_{LF}) - V_F\right], \\ U_{23} &= -\frac{1}{V_O}\left[L_S(-\beta x_1 - \alpha_2 x_2 + \dot{I}^*_{LS}) - V_S\right], \end{aligned} \tag{8}$$

the current error dynamics are rewritten as a linear time-invariant (LTI) dynamical system of the form

$$\begin{bmatrix} \dot{x}_1 \\ \dot{x}_2 \end{bmatrix} = \begin{bmatrix} -\alpha_1 & \beta \\ -\beta & -\alpha_2 \end{bmatrix} \begin{bmatrix} x_1 \\ x_2 \end{bmatrix}. \tag{9}$$

Note that, if $\beta = 0$, the system (9) results in an uncoupled LTI system, where α_1 and α_2 represents the poles of the current loop and need to be positive constants to ensure the asymptotic stability of the origin. On the other hand,

the stability of (9) can be ensured by two methods. For instance, the characteristic polynomial of (9) is obtained as $P_x(\lambda) = \lambda^2 + (\alpha_1 + \alpha_2)\lambda + (\beta^2 + \alpha_1\alpha_2)$, from where is possible to assign a desired root locus by selecting proper values for the tuning gains. Since the control objectives of the inner loop are

$$\lim_{t\to\infty} x_1(t) = 0, \quad \lim_{t\to\infty} x_2(t) = 0, \tag{10}$$

then, a candidate Lyapunov function $V_1 : \mathbb{R}^2 \to \mathbb{R}$ can be proposed as

$$V_1(x_1, x_2) = \frac{1}{2}(x_1^2 + x_2^2). \tag{11}$$

After some computations, the time derivative of V_1 along the trajectories of (9) is

$$\dot{V}_1 = -\alpha_1 x_1^2 - \alpha_2 x_2^2, \tag{12}$$

which result is to be a negative-definite function, assuring the asymptotic stability of the origin of (9); consequently, $I_{LF} = I_{LF}^*$ and $I_{LS} = I_{LS}^*$ as $t \to \infty$. Observe that, the control laws in (8) require that the output voltage V_O remain nonzero for all time. This restriction is nonconservative since, in practice, V_O is always positive and higher than the fuel cell voltage. Observe that there is no restriction over β; however, is selected as a positive constant. Furthermore, β improves the loop performance, since its selection establish a level of interconnection between both duty cycles.

B. Voltage controller (Outer loop)

Assuming current errors x_1 and x_2 equal to zero, then $I_{LF} = I_{LF}^*$ and $I_{LS} = I_{LS}^*$, therefore the *slow* dynamics of (2) are given by

$$\begin{aligned} C_F\dot{V}_F &= \left(\frac{V_F - c}{a}\right)^{1/b} - I_{LF}^*, \\ C_S\dot{V}_S &= -I_{LS}^*, \\ C_O\dot{V}_O &= I_{LF}^*\frac{V_F}{V_O} + I_{LS}^*\frac{V_S}{V_O} - I_O, \end{aligned} \tag{13}$$

where I_{LS}^* and I_{LF}^* are control inputs to be designed. Afterwards, define the fuel cell stack, supercapacitor and output voltage errors as

$$\begin{aligned} x_0 &:= V_F - V_F^*, \\ x_3 &:= V_S - V_S^*, \\ x_4 &:= V_O - V_O^*. \end{aligned} \tag{14}$$

Consequently, considering the above error definitions, the error dynamics of (13) can be rewritten as

$$\begin{aligned} \dot{x}_0 &= -h(x_0), \\ \dot{x}_3 &= -\frac{I_{LS}^*}{C_S}, \\ \dot{x}_4 &= \frac{1}{C_O}\left[I_{LF}^*\frac{V_F}{V_O} + I_{LS}^*\frac{V_S}{V_O} - I_O\right] \end{aligned} \tag{15}$$

where

$$h(x_0) = \frac{1}{C_F}\left[-\left(\frac{x_0 + V_F^* - c}{a}\right)^{1/b} + I_{LF}^*\right]. \tag{16}$$

Note that $h(x_0)$ is an odd function which satisfies $h(0) = 0$ and $h(x_0)x_0 > 0$ when $x_0 \neq 0$. The last feature will be exploited later in the stability analysis [22]. Similar to the inner control loop design, if the current references are selected as

$$\begin{aligned} I_{LS}^* &= C_S\left[\gamma_1 x_3 - \delta x_4\right], \\ I_{LF}^* &= \frac{V_O}{V_F}\left[C_O(-\delta x_3 - \gamma_2 x_4) - I_{LS}^*\frac{V_S}{V_O} + \frac{V_O}{R}\right], \end{aligned} \tag{17}$$

then, the voltage error dynamics are rewritten as

$$\begin{aligned} \dot{x}_0 &= -h(x_0), \\ \begin{bmatrix} \dot{x}_3 \\ \dot{x}_4 \end{bmatrix} &= \begin{bmatrix} -\gamma_1 & \delta \\ -\delta & -\gamma_2 \end{bmatrix}\begin{bmatrix} x_3 \\ x_4 \end{bmatrix}. \end{aligned} \tag{18}$$

Now, to analyze the stability of (18) and to fulfill the control objectives

$$\lim_{t\to\infty} x_0(t) = 0, \quad \lim_{t\to\infty} x_3(t) = 0, \quad \lim_{t\to\infty} x_4(t) = 0, \tag{19}$$

of the voltage loop, a continuously differentiable candidate Lyapunov function $V_2 : \mathbb{R}^3 \to \mathbb{R}$ is proposed as follows

$$V_2(x_0, x_3, x_4) = \int_0^{x_0} h(y)\,dy + \frac{1}{2}(x_3^2 + x_4^2), \tag{20}$$

which after some computations, the time derivative of V_2 along the trajectories of (18) is

$$\dot{V}_2 = -h(x_0)^2 - \gamma_1 x_3^2 - \gamma_2 x_4^2, \tag{21}$$

which results to be a negative-definite function if γ_1 and γ_2 are selected as positive constants; thus, assuring asymptotic stability of the origin of (18), and consequently $V_F = V_F^*$, $V_S = V_S^*$ and $V_O = V_O^*$ as $t \to \infty$. The tuning gain δ has been selected to be a positive constant for practical purposes. Note that, this gain introduces the interconnection of the errors x_4 and x_3 between the current references to improve the performance of the loop. Besides, the online computation of the current references (17) does not requires the knowledge of V_F^* (which coincides with $\bar{V}_F$, whose value is not known in practice), since the dynamics of x_0 does not need to be controlled. On the other hand, about I_{LF}^*, it is required the knowledge of $I_O = V_O/R$, which is unknown. To overcome this issue, a load estimator design is considered in the following.

C. I&I adaptation law for load estimation

In this part, an adaptation law based on immersion and invariance (I&I) theory is detailed. The objective is to generate the estimation $\hat{R}$ of R and to use in a *certainty-equivalent* way this estimation in the current reference generator (17). This approach has been widely reported in the open literature to design asymptotically stabilizing laws, state observers and parameter estimators for nonlinear systems [13], [14], [23], [24]. In the following, the methodology used to design the

adaptation scheme is shown in detail. To begin with, consider $\theta = 1/R$ as the unknown parameter of (2), thus the output voltage state equation is rewritten as $\dot{V}_O = \frac{1}{C_O}(1-U_1)I_L + \frac{1}{C_O}I_{LS}U_{23} - \frac{1}{C_O}\theta V_O$. Then, the estimation error of θ is defined as following

$$z = \hat{\theta} - \theta, \tag{22}$$

where, accordingly to I&I theory, $\hat{\theta}$ is formed by two terms; an integral term ξ and a proportional term $\eta(V_O)$, this is $\hat{\theta} = \xi + \eta(V_O)$. Assuming that θ is an unknown constant parameter, the time derivative of the estimation error (22) results in

$$\begin{aligned}\dot{z} = \dot{\xi} + \frac{\partial \eta}{\partial V_O}\dot{V}_O = \dot{\xi} + \frac{1}{C_O}\frac{\partial \eta}{\partial V_O}\Big((1-U_1)I_{LF} \\ + I_{LS}U_{23} - \theta V_O\Big).\end{aligned} \tag{23}$$

From (22), it is known that $\theta = \hat{\theta} - z$, then (23) is rewritten as

$$\begin{aligned}\dot{z} = \dot{\xi} + \frac{1}{C_O}\frac{\partial \eta}{\partial V_O}\Big((1-U_1)I_{LF} + I_{LS}U_{23} \\ - (\xi + \eta(V_O) - z)V_O\Big).\end{aligned} \tag{24}$$

Splitting (24) with respect to the error variable z, it is found that

$$\begin{aligned}\dot{z} = &\dot{\xi} + \frac{1}{C_O}\frac{\partial \eta}{\partial V_O}\Big((1-U_1)I_{LF} + I_{LS}U_{23} \\ &- (\xi + \eta(V_O))V_O\Big) + \frac{1}{C_O}\frac{\partial \eta}{\partial V_O}zV_O,\end{aligned} \tag{25}$$

therefore, the adaptation law is selected as

$$\begin{aligned}\dot{\xi} = -\frac{1}{C_O}\frac{\partial \eta}{\partial V_O}\Big((1-U_1)I_{LF} \\ + I_{LS}U_{23} - (\xi + \eta(V_O))V_O\Big),\end{aligned} \tag{26}$$

such that the dynamics of the estimation error is transformed into $\dot{z} = \frac{1}{C_O}\frac{\partial \eta}{\partial V_O}V_O z$. Then, if $\eta(V_O) = -C\sigma V_O$, with $\sigma > 0$, results in $\partial\eta/\partial V_O = -C\sigma$, and the last expression for $\dot{z}$ is simplified as $\dot{z} = -\sigma V_O z$. From the last expression, a candidate Lyapunov function $W(z) = \frac{1}{2}z^2$ is proposed. The time derivative of W along the error trajectory is computed as $\dot{W} = -\sigma V_O z^2$, since by definition V_O is always positive, then $\dot{W}$ is always negative and it is possible to state that $z(t) \to 0$ when $t \to \infty$, consequently $\theta = \hat{\theta}$.

IV. Simulation Results

The performance of the proposed multi-loop adaptive control scheme in closed-loop with the average model of the HES (see (2)) under load step changes (R varies from a nominal load of 5 Ω to 10 Ω every 20 seconds) is evaluated using numerical simulation carried out in Simulink/Matlab using the solver ode 23tb (stiff/TR-BDF2) and a variable integration step whit relative and absolute tolerance of 1×10^{-6}. All system parameters are gathered in Table I. Note that, based on the analysis of section 3, all the gains are selected to ensure the best response of the closed loop system. For instance, α_1, α_2 and β, are related to the current loop; meanwhile, γ_1, γ_2 and δ, are related to the voltage loop. The FC Nexa power module considered in here, has 40.7 V open circuit voltage and maximum power of 1.2 kW. The maximum acceptable current ripple is 35% peak-to-peak at a switching frequenzy of 120 Hz. The SC bank consists of 12 capacitors in series. Each capacitor of 150 F and a nominal voltage of 2.7 V, resulting in a total capacitance of 12.5 F. Note that, V_S^* is set to 24 V to avoid any overcharge in the capacitor. First of all, Fig. 4 (a) depicts the FC voltage, the inductor current tracking and the MSS voltage regulation. Observe that V_F varies smoothly from 28 V (at nominal load) to 34 V, every load change. On the other hand, I_{LF} goes from 15.5 A to 7.5 A. It is observed a proper tracking; therefore, the lifetime of the FC is not affected. Lastly, the proposed controller ensures the output voltage regulation at 48 V despite load changes. It is noticeable that, in less than 5 s after the load variation, V_O returns to the nominal value. Due to the large load changes, there exists small overshoot around 48 V. The SC current tracking and voltage regulation are shown in Fig. 4 (b). It is noticeable that each load transition, I_{LS} is around $\pm$ 10 A to compensate for the load changes. Otherwise, the SC current is zero. On the other hand, each load transition, the SC voltage is (dis)charged around $\pm$ 0.5 V over 24 V, and the voltage reference level is reached after 10 s. The control signals are given in Fig. 4 (c). Meanwhile, U_1 smoothly moves from 0.39 to 0.3 to compensate the load changes, U_{23} abruptly changes to ensure a proper SC current tracking. Finally, Fig. 4 (c), shows the load estimation. Note that, the convergence rate of the estimator has been chosen to be slow in purpose ($\sigma = 0.01$), since this is directly related to the slope of the FC current reference. As depicted in Fig. 4 (c), the convergence rate of the estimation increaser, as σ increases as well.

TABLE I
System parameters and controller gains.

Parameter	Value	Gains	Value
V_O^*	48 V	a	-2.219
C_O	1.88 mF	b	0.5848
R	5-10 Ω	c	40.45
C_F	11.2 mF	α_1	10x10^3
L_F	135 μH	α_2	10x10^3
L_S	135 μH	β	1.5x10^3
C_S	12.5 F	δ	2.5
		γ_1	0.5
		γ_2	10x10^3

V. Conclusion

The problem of controlling the output voltage regulation of the MSS under study using an adaptive multi-loop nonlinear control scheme has been addressed. The system consists of an FC and an SC as the primary and auxiliary sources, respectively. Both sources are connected to a DC-bus through a boost and bidirectional converters. The control methodology was focused on the design of two feedback loops; the inner loop for current tracking and the external loop for voltage regulation, meanwhile the stability proof relies upon Lyapunov stability analysis. Moreover, the robustness of the voltage loop has been improved introducing an I&I load estimator, which

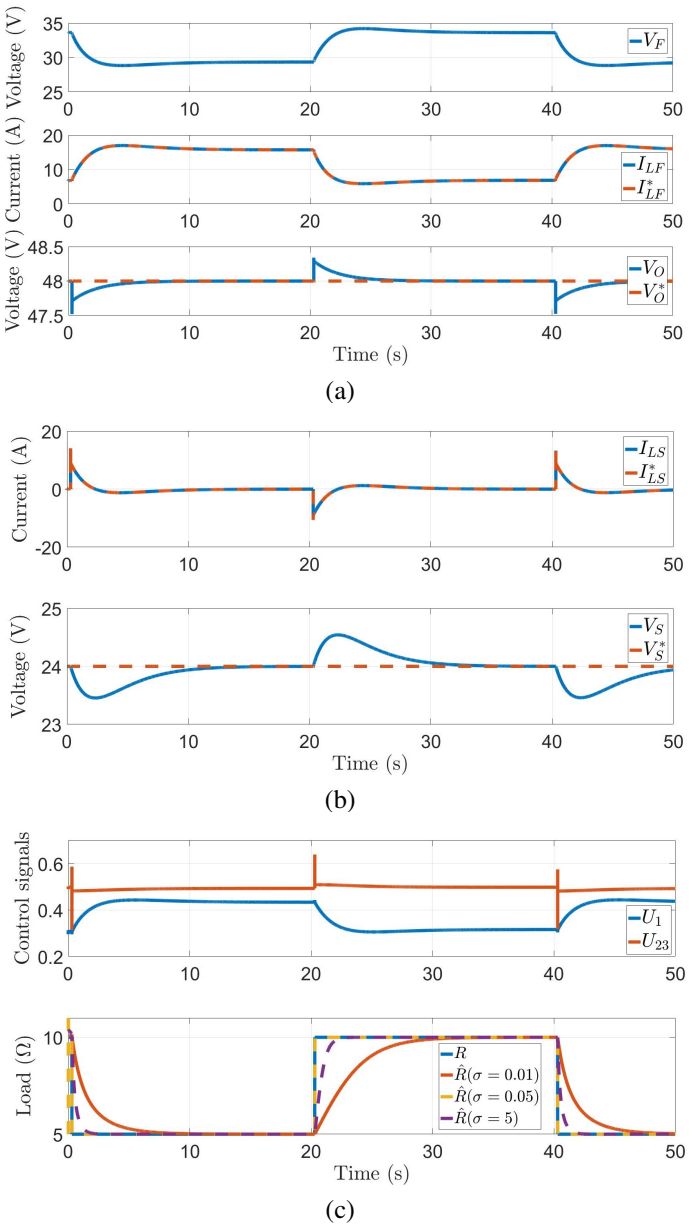

Fig. 4. Closed-loop time histories of the MSS under load step changes. (a) FC voltage, Boost inductor current and MSS output voltage. (b) Buck-Boost inductor current and SC voltage. (c) Control signals and Load estimation.

is useful to dictate the rate of change of the FC current and preventing dangerous operation. A precise regulation, tracking and robust behavior concerning large unknown load and FC voltage variations were successfully proven. Future research is toward to realize a practical implementation; therefore, the improvement and performance evaluation of the control strategy under measurement noise, external disturbances and parametric uncertainty are mandatory.

ACKNOWLEDGMENT

Yuz A. Zúñiga-Ventura would like to thank the Mexican Consejo Nacional de Ciencia y Tecnología (CONACyT) for the scholarship No. 279109, and the Consejo Potosino de Ciencia y Tecnología (COPOCyT) for the economical support.

REFERENCES

[1] M. Nehrir and C. Wang, *Modeling and control of fuel cells: distributed generation appliactions*. IEEE Press, 2009.

[2] C. Kunusch, P. Puleston, and M. Mayosky, *Sliding-Mode Control of PEM Fuel Cells*. Springer, 2012.

[3] L. H. Diaz-Saldierna, J. Leyva-Ramos, D. Langarica-Cordoba, and J. A. Morales-Saldana, "Control strategy of switching regulators for fuel-cell power applications," *IET Renewable Power Generation*, vol. 11, no. 6, pp. 799–805, 2017.

[4] A. Amamou, M. Kandidayeni, L. Boulon, and S. Kelouwani, "Real time adaptive efficient cold start strategy for proton exchange membrane fuel cells," *Applied Energy*, vol. 216, pp. 21 – 30, 2018. [Online]. Available: http://www.sciencedirect.com/science/article/pii/S0306261918301909

[5] H. E. Fadil and F. Giri, "Modeling and nonlinear control of a fuel cell/supercapacitor hybrid energy storage system for electric vehicles," *IEEE Transactions on Vehicular Technology*, pp. 3011–3018, September 2014.

[6] X. Song, J. Deng, D. Xu, and W. Yan, "Generic model control for hybrid energy storage system in electric vehicles," pp. 7151–7156, Oct 2017.

[7] P. Thounthong, S. Rael, and B. Davat, "Control strategy of fuel cell and supercapacitors association for a distributed generation system," *IEEE Transactions on Industrial Electronics*, vol. 54, no. 6, pp. 3225–3233, December 2007.

[8] M. Hilairet, M. Ghanes, and O. Béthoux, "A passivity-based controller for coordination of converters in a fuel cell system," *ELSEVIER Control ENgineering Practice*, vol. 21, no. 8, pp. 1097–1109, May 2013.

[9] F. Yang, B. Sheng, and Y. Fu, "Energy management for fuel cell-supercapacitor hybrid system using passivity-based controller with multi-equilibrium states," pp. 000 511–000 516, Nov 2015.

[10] H. Yuan and L. Dung, "A hybrid fuel cell-battery power system," pp. 4096–4102, Oct 2014.

[11] L. Hu, Y. J. Kim, J. M. Kwon, and H. J. Cho, "A novel control strategy for dc/dc power converter of fuel cell hybrid system," pp. 2765–2770, Nov 2010.

[12] A. Zabetian-Hosseini, Y. Sangsefidi, and A. Mehrizi-Sani, "Model predictive control of a fuel cell-based power unit," pp. 4961–4966, Oct 2017.

[13] D. Langarica-Córdoba, R. Ortega, and D. Casagrande, "Transient stabilization of multimachine power systems: Towards a global decentralized solution," *European Journal of Control*, vol. 26, pp. 44 – 52, 2015.

[14] D. Langarica Córdoba and R. Ortega, "An observer-based scheme for decentralized stabilization of large-scale systems with application to power systems," *Asian Journal of Control*, vol. 17, no. 1, pp. 124–132, 2015.

[15] M. Ayad, M. Becherif, A. Henni, A. Aboubou, M. Wack, and S. Laghrouche, "Passivity-based control applied to {DC} hybrid power source using fuel cell and supercapacitors," *Energy Conversion and Management*, vol. 51, no. 7, pp. 1468 – 1475, 2010.

[16] Amin, R. T. Bambang, A. S. Rohman, C. J. Dronkers, R. Ortega, and A. Sasongko, "Energy management of fuel cell/battery/supercapacitor hybrid power sources using model predictive control," *IEEE Transactions on Industrial Informatics*, vol. 10, no. 4, pp. 1992–2002, Nov 2014.

[17] J. H. Jung, S. Ahmed, and P. Enjeti, "Pem fuel cell stack model development for real-time simulation applications," *IEEE Transactions on Industrial Electronics*, vol. 58, no. 9, pp. 4217–4231, Sept 2011.

[18] C. Restrepo, T. Konjedic, A. Garces, J. Calvente, and R. Giral, "Identification of a proton-exchange membrane fuel cell's model parameters by means of an evolution strategy," *IEEE Transactions on Industrial Informatics*, vol. 11, no. 2, pp. 548–559, April 2015.

[19] S. C. Chapra and R. P. Canale, *Numerical Methods for Engineers*. New York, NY: McGraw-Hill, 2010.

[20] Y. A. Zúniga-Ventura, D. Langarica-Córdoba, and J. Leyva-Ramos, "Adaptive backstepping control for a fuel cell/boost converter system," *IEEE Journal of Emerging and Selected Topics in Power Electronics*.

[21] S. N. M., O. Tremblay, and L. A. Dessaint, "A generic fuel cell model for the simulation of fuel cell vehicles," in *2009 IEEE Vehicle Power and Propulsion Conference*, Sept 2009, pp. 1722–1729.

[22] H. K. Khalil, *Nonlinear systems*, 3rd ed. Prentice hall, 2002.

[23] A. Astolfi, D. Karagiannis, and R. Ortega, *Nonlinear and adaptive control with applications*. Springer Science & Business Media, 2007.

[24] A. Astolfi and R. Ortega, "Immersion and invariance: a new tool for stabilization and adaptive control of nonlinear systems," *IEEE Transactions on Automatic Control*, vol. 48, no. 4, pp. 590–606, April 2003.